Advances in SQUID-detected magnetic resonance force microscopy

Wit, M. de

8

Double-magnet cantilevers for increased magnetic field gradients

Ever since its first conception, the goal of MRFM was to reach levels of sensitivity sufficient to measure the properties of a single nuclear spin [1]. One of the approaches to increase the sensitivity of MRFM is to increase the spin signals by increasing the magnetic field gradients. In this chapter, we motivate this approach, and describe our attempt to increase the magnetic field gradient in such a way that it requires minimal change to the experimental setup, and reduces the effects of potential drawbacks.

8.1 Introduction

There has been a wide variety of methods to maximize the magnetic field gradients in MRFM. The standard approach of growing a magnetic structure on top of the RF source is widely used and has been very successful [16, 57, 197]. The fabrication of these structures is relatively straightforward, and by creating sharp edges, very large field gradients of up to 6 MT/m can be achieved using a variety of magnetic materials, such as dysprosium and iron-cobalt. The most extreme example of this approach was the utilization of a commercial disk drive write head, resulting in a record magnetic field gradient of 28 MT/m, with the added advantage of dynamic control of the gradient with frequencies up to 1 GHz [42]. However, this approach has the drawback of a complex resonant slice shape, and positioning the sample to within 100 nm of these structures can be challenging.

A more innovative approach of creating the magnetic field gradients is by using a current-focusing field gradient source (CFFGS), in which a constriction in a current-carrying wire is used to generate time-dependent field gradients of up to 1 MT/m, but at the cost of significant dissipation [17, 114, 198]. The maximum field gradients are limited by the breakdown current density in the wire. Once again, the experiment has to be performed very close (within 50 nm) to the wire.

The methods described above are all based on the sample-on-tip approach for MRFM. There has also been work focused on the magnet-on-tip approach. Micron-sized SmCo-particles have been used to generate gradients of up to 0.5 MT/m [19, 63, 199]. Higher field gradients can be achieved by using focused ion beam milling to shape magnetic particles [200–202] or using e-beam lithography [203], with the record set at 5.4 MT/m [41]. A big issue for all of these approaches is the positioning of the magnetic tip with respect to the sample. Furthermore, due to our SQUID-based detection, the problem is intensified as we are even incapable of detecting the cantilever motion at all when the cantilever is not positioned close enough to the pickup loop.

In an attempt to evade this issue, we have decided to combine two NdFeB magnets with different radii on the same cantilever: a small one to create higher field gradients than our group has achieved in the past, and a large one to have a high coupling to the SQUID-based detection system, which eases positioning and reduces the detection noise. This approach requires minimal changes to the experimental setup, and reduces the effects of potential drawbacks. We calculate the expected magnetic fields originating from these new cantilevers, and how this influences the flux coupling to the pickup loop. We end the chapter by analyzing how the spin-induced dissipation

is affected by the higher magnetic field gradients.

8.2 Intuition about magnetic field gradients

The purpose of this section is to create some intuition about how the signals in MRFM scale with the size of the magnet used to generate the magnetic field gradient. In this section we will use the following simplifications:

- To be completely correct one has to always consider only the component of the force in the soft-direction of the cantilever, which in our case is the horizontal direction parallel to the magnetization of the magnet. However, in order to be able to gain some insight in the various scaling laws, we will consider the magnetic field gradient in the radial direction instead. This simplification will be justified in Sec. 8.5.
- We neglect the dynamics of the spin in the cantilever's magnetic field, assuming that the moment of the spin $\boldsymbol{\mu_s}$ is always perfectly aligned with the field. In that case, the interaction between the spin and the magnetic field can be determined from the interaction energy $E = -(\boldsymbol{\mu}_\mathrm{s} \cdot \boldsymbol{B})$, instead of from the full analysis by De Voogd et al. [52].

An intuitive picture of how the radius of the magnet influences the expected signals is given by Garner [204]. When a single spin with magnetic moment $\boldsymbol{\mu}_\mathrm{s}$ is placed in a magnetic field $\boldsymbol{B}$ originating from the magnet on the tip of the cantilever, this creates a force between the spin and the cantilever, given by:

$$\boldsymbol{F} = \nabla (\boldsymbol{\mu}_\mathrm{s} \cdot \boldsymbol{B}) = \boldsymbol{\mu}_\mathrm{s} \cdot \nabla \boldsymbol{B} \tag{8.1}$$

This force induces a shift of the stiffness of the cantilever:

$$k_\mathrm{s} = \boldsymbol{\mu}_\mathrm{s} \cdot \nabla^2 \boldsymbol{B} \tag{8.2}$$

which results in a measurable frequency shift according to

$$\Delta f = \frac{1}{2} \frac{k_\mathrm{s}}{k_0} f_0 \tag{8.3}$$

To use these equations, we need to know the distribution of the magnetic field originating from the magnet. As discussed in Ch. 2, we can describe the spherical

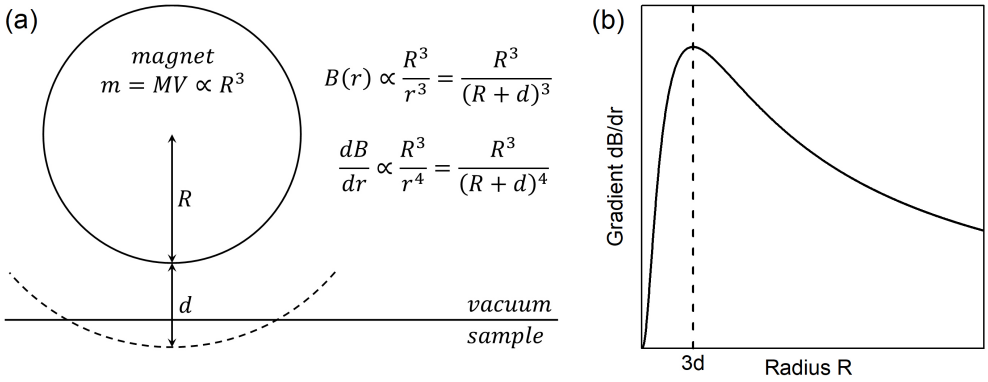

Figure 8.1: (a) Schematic of a magnet with radius R positioned above a sample with a resonant slice at a distance d from the surface of the magnet. (b) Calculated gradient versus radius of the magnet for a given d. The gradient is maximal for $R = 3d$.

magnet at the tip of the cantilever as a magnetic dipole with magnetic moment $\boldsymbol{m}$, for which the field is given by [146]

$$\boldsymbol{B}(\boldsymbol{r}) = \frac{\mu_0}{4\pi}\frac{\boldsymbol{m}}{r^3}\left[3\left(\hat{\boldsymbol{m}}\cdot\hat{\boldsymbol{r}}\right)\hat{\boldsymbol{r}} - \hat{\boldsymbol{m}}\right] \tag{8.4}$$

Here $r = |\boldsymbol{r}|$ is the distance to the center of the magnet positioned at the origin, which can be rewritten as $r = R + d$, with R the radius of the magnet and d the distance between the surface of the magnet and the resonant slice. The situation is sketched in Fig. 8.1(a). The magnetic moment, in turn, can be rewritten in terms of the saturation magnetization $M = \boldsymbol{B}_\mathrm{r}/\mu_0$ and the volume V of the spherical magnet[1]:

$$\boldsymbol{m} = \frac{\boldsymbol{B}_\mathrm{r}}{\mu_0}V = \frac{4\pi}{3}\frac{1}{\mu_0}\boldsymbol{B}_\mathrm{r}R^3 \tag{8.5}$$

Thus, $\boldsymbol{B} \propto R^3/(R+d)^3$. Considering this, the first derivative of the magnetic field, for simplicity calculated in the radial direction, then scales as

$$\frac{\partial \boldsymbol{B}}{\partial r} \propto \frac{R^3}{r^4} = \frac{R^3}{(R+d)^4} \tag{8.6}$$

Let us now consider the implications of these equations for maximizing the magnetic field gradient, and thereby the MRFM signals. First, imagine that we can perform our experiment right at the surface of the magnet, so $d = 0$. Then the gradient scales as R^{-1}, and we should take the smallest possible magnet to obtain the largest magnetic field gradient.

[1] For our magnetic material, NdFeB, B_r is equal to 1.15 - 1.3 T [51, 59]

However, in practice it is not possible to measure so close to the surface of the magnet, as non-contact friction reduces the sensitivity of the experiment [51, 52, 68]. When we therefore demand that d is a constant value larger than 0, we can maximize the gradient to find that for a given d there is an optimal radius $R = 3d$ [204]. A plot of the gradient is shown in Fig. 8.1(b). When the radius is much smaller than $3d$, the gradient roughly scales with R^3, as the decreasing radius reduces the magnetic moment. So, for measurements where $d > R/3$, one would be better off using a larger magnet. On the other hand, when the radius is much larger than $3d$, the gradient scales with R^{-1}, and a smaller magnet would give a higher signal per spin. So, decreasing the size of the magnetic particle is only beneficial when the experiment can be performed within $d < R/3$.

There is a second important aspect to consider, namely the total MRFM signal. Let's say that we are always measuring at a distance d that is proportional to the radius. In other words, when the radius is increased, the distance between the magnet and the sample is increased proportionally. Then the force per spin increases as the size of the magnetic particle is reduced, proportional to R^{-1}. However, the volume of the resonant slice, and thus the number of spins within it, increases with the size of the magnetic particle, proportional to R^3. Therefore, even though the signal per spin and the volume sensitivity are improved, the total MRFM signal in the experiment decreases when a smaller magnet is used.

8.3 Signal-to-noise ratio

As usual in MRFM, the right experimental parameters depend on the specific experiment in mind. A measurement based on using spins to drive the amplitude of the cantilever, a so-called force measurement, has different optimal parameters than a frequency shift measurement.

We start from the assumption that our experiment is thermally limited, i.e. the dominant noise factor is the thermal force noise, given by

$$S_{\mathrm{F}} = 4k_{\mathrm{B}}T\Gamma \tag{8.7}$$

with $\Gamma = k/(\omega_0 Q)$ the damping of the cantilever. The signal-to-noise ratio (SNR) for a force experiment on a single spin with magnetic moment μ_s is then given by

$$\mathrm{SNR}_{\mathrm{F}} = \mu_{\mathrm{s}} \frac{\partial \boldsymbol{B}}{\partial x} \left(4k_{\mathrm{B}}T\Gamma\ BW\right)^{-\frac{1}{2}} \tag{8.8}$$

with BW the bandwidth of the measurement[2].

For a frequency shift measurement we want to find the frequency noise. First, we can calculate the noise in the stiffness of the cantilever using Hooke's law as transfer function, leading to

$$S_{\mathrm{k}} = \frac{S_{\mathrm{F}}}{A^2} = \frac{4k_{\mathrm{B}}T\Gamma}{A^2} \tag{8.9}$$

with A the rms amplitude of the cantilever motion. From this, we can find the frequency noise using

$$S_{\delta \mathrm{f}_0}(f) = \left(\frac{1}{2}\frac{f_0}{k_0}\right)^2 S_{\mathrm{k}} = \frac{k_{\mathrm{B}}T\Gamma f_0^2}{k_0^2 A^2} \tag{8.10}$$

Note that this equation is only valid for $f \gg f_0/(2Q)$. We can combine this with Eqs. 8.2 and 8.3 to find the frequency shift SNR:

$$\mathrm{SNR}_{\delta \mathrm{f}_0} = \frac{f_0}{2}\frac{\mu_{\mathrm{s}}}{k_0}\frac{\partial^2 \boldsymbol{B}}{\partial x^2}\left(\frac{k_{\mathrm{B}}T\Gamma f_0^2\ BW}{k_0^2 A^2}\right)^{-\frac{1}{2}} \tag{8.11}$$

Using Eqs. 8.8 and 8.11, we can compare the relative signal-to-noise ratios of the two experiments for different experimental parameters when both experiments are operated in the thermal limit:

$$\frac{\mathrm{SNR}_{\mathrm{F}}}{\mathrm{SNR}_{\delta \mathrm{f}_0}} \propto \frac{R_0}{A} \tag{8.12}$$

Here we assume the experiments are performed at the optimal height as described in Sec. 8.2. Frequency shift experiments become more interesting for smaller magnets and large driving amplitudes. However, given that the radius of the magnetic particle is on the order of several micrometers, and that the driven cantilever amplitude is roughly 1 - 100 nm, direct force measurements remain more sensitive for our range of experimental parameters.

8.4 Fabrication of double-magnet cantilevers

Based on considerations from the previous sections, we have fabricated MRFM cantilevers that combine a small diameter particle at the tip of the cantilever for a high

[2] Here we assume a single-shot experiment (no averaging) where we reduce the spin magnetic moment to zero, as would be the case in a saturation experiment.

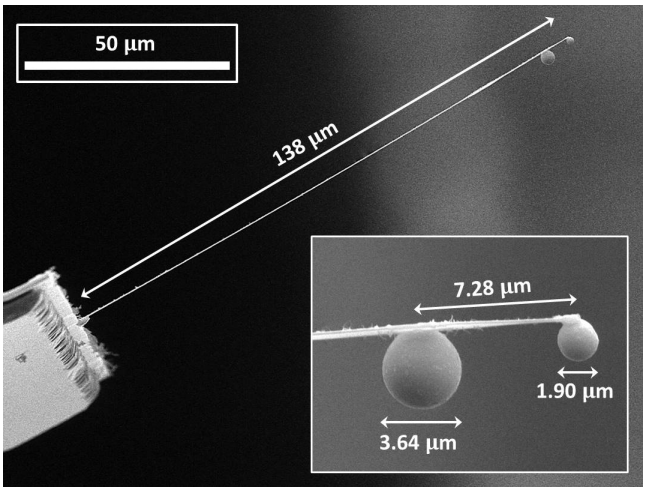

Figure 8.2: Scanning electron microscope image of the double magnet cantilever. The inset shows a zoom on the tip of the cantilever.

field gradient with a larger diameter particle a bit higher up the cantilever to maintain a high coupling strength to the SQUID. In selecting the appropriate combination of cantilever and magnet sizes, a trade-off is made between the sensitivity, for which a low stiffness is required, and keeping the resonance frequency high enough to stay within the effective range of the vibration isolation. We aim for finished cantilevers with a resonance frequency close to 3 kHz, similar to the conventional cantilevers in our group.

In total, three cantilevers were made with slightly different parameters. In the remainder of this chapter, we will base our calculations on the parameters of one of these finished double-magnet cantilevers, which is shown in Fig. 8.2. This new cantilever has a length of 138 µm and carries two magnets: at the very end, a small magnet with radius $R_1 = 0.95$ µm, and at about 7.3 µm from the tip a second larger magnet with a radius $R_2 = 1.82$ µm. The magnets are attached to the cantilever using the same method as described in Sec. 2.3.

The resonance frequency of the cantilever can be calculated using the familiar equation $\omega_0^2 = k_0/m$, but with a modified effective mass which takes into account the new mass distribution $\rho(l)$. When we assume the magnetic particles to be point masses, we find for the effective mass

$$m = \int_0^l \frac{x^2}{l^2}\rho(x)dx = m_1\frac{x_1^2}{l^2} + m_2\frac{x_2^2}{l^2} + \frac{\rho_{\mathrm{Si}}lwt}{4}, \tag{8.13}$$

with m_1 and m_2 the masses of the small and large magnets, respectively, and x_1

and x_2 their respective positions measured from the base of the cantilever. The last term represents the effective mass of the silicon cantilever itself, with ρ_{Si} the density of silicon[3]. Using this equation with the parameters obtained from Fig. 8.2, the calculated natural frequency of the double-magnet cantilever is 3086.7 Hz, very close to the 3085.1 Hz measured at 4 K.[4]

8.5 Magnetic field distribution

The main purpose of the large top magnet is to increase the coupling strength between the cantilever and the SQUID, as will be discussed in Sec. 8.6. However, a potential downside is that the large magnet might have an effect on the field at the position of the sample, thereby complicating the shape of the resonant slice. To check this, we calculate the total magnetic field resulting from both particles. A contour plot of the field distribution is shown in Fig. 8.3(a). The figure shows that the field of the large top particle falls off sufficiently quick that the amplitude and shape of the resonant slices (constant B_0) below the bottom magnet are hardly affected, allowing us to do our simulations using a simple single dipole model. This is confirmed in figure 8.3(b), where we compare the magnitude of the field directly below the bottom magnet with and without the top magnet. We find that at small heights, where all of the experiments are performed, the magnitude of the magnetic field is unaltered by the presence of the large upper magnet.

Of course, the main goal of going for smaller magnetic particles is to increase the magnetic field gradient. Fig. 8.4(a) shows a contour plot of the derivative of the magnetic field in the X-direction for a magnet with a radius of 0.95 μm[5]. As expected, the derivative is zero directly below the magnet, but increases to values of several hundred mT/μm at positions right in front of or behind the magnet.

A cross section of the contour plot along the line Z = $R_0/3$ is show in Fig. 8.4(b), calculated for two magnets with different radii of 0.85 μm and 1.9 μm. From this image, we find the following: First of all, the maximum field gradient is indeed inversely proportional to the radius of the magnet; secondly, the distance to the optimum of ∂B/∂x scales with the radius of the magnet, so a smaller particle reduces the effective field of view of the MRFM. Both of these observations match the predictions from Sec. 8.3 where we looked at the radial component of the magnetic field gradient, showing

[3] $\rho_{\mathrm{Si}} = 2330$ kg/m^3 and $\rho_{\mathrm{NdFeB}} = 7400$ kg/m^3.
[4] Note: this calculation is only valid for the fundamental mode.
[5] reminder: the Z-direction is the vertical direction along the axis of the cantilever, and the X-direction is pointed along the soft direction of the cantilever and the magnetization of the magnets.

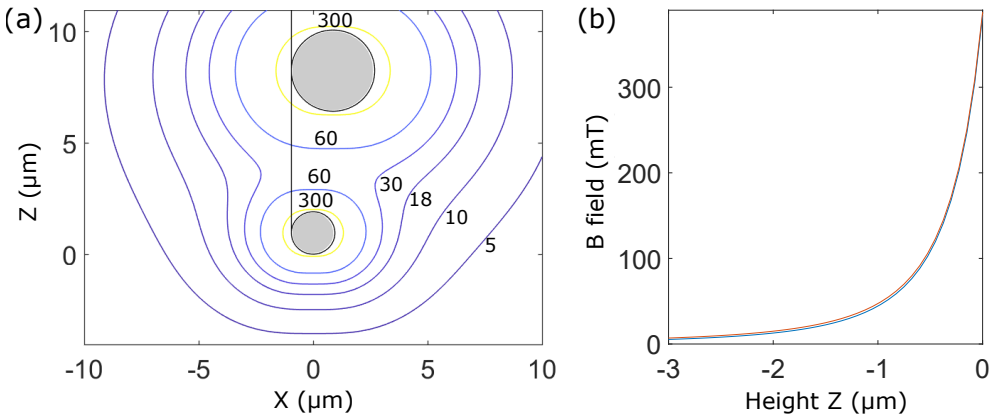

Figure 8.3: (a) Contour plot of the magnetic field distribution around the new cantilever (radii 0.95 µm and 1.82 µm). The gray circles indicate the positions of the magnets. The labels indicate the magnitude of the field (mT) for the different contour lines. (b) B-field versus the distance between the sample and the surface of the magnet for a single magnet (blue) and the double magnet (red) configurations, calculated directly below the magnet.

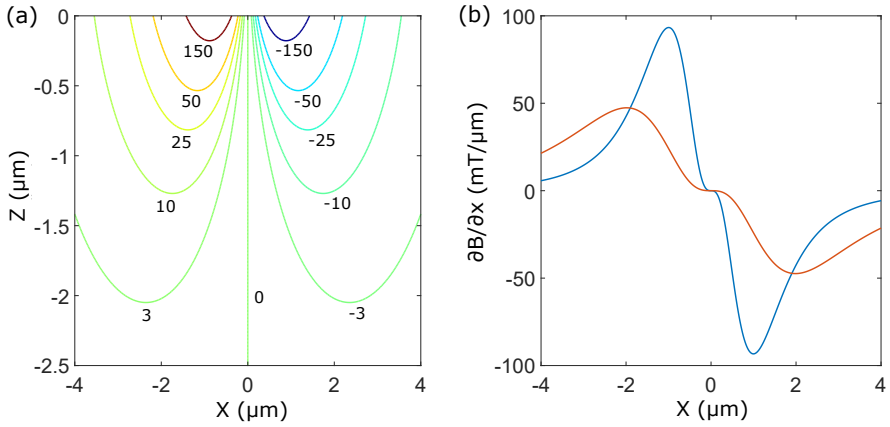

Figure 8.4: (a) Contourplot of $\partial B/\partial x$ in the $Y = 0$ plane for a magnet with radius 0.95 µm. The labels indicate the magnitude of $\partial B/\partial x$ in units mT/µm. The surface of the magnet is located at $Z = 0$. (b) Cross-section of Fig. (a) for two different magnets, one with radius 0.95 µm (blue) and the other with radius 1.9 µm (red), along $Z = R_0/3$ (following Garner). As predicted, the magnitude of $\partial B/\partial x$ scales with the inverse of the radius of the magnet, while the distance between the center of the magnet and the optimum of $\partial B/\partial x$ scales linearly with the radius.

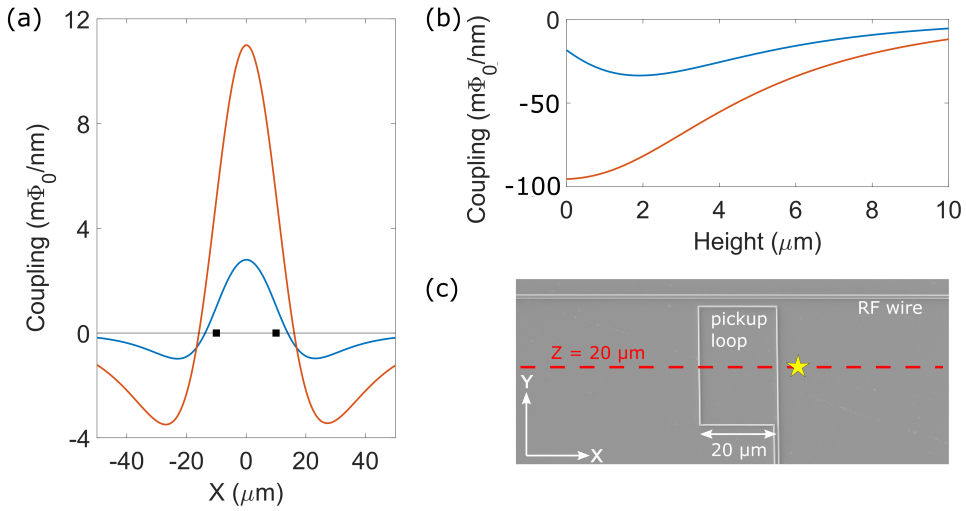

Figure 8.5: Calculation of the improved coupling of the double magnet cantilevers (solid red) compared to a single magnet cantilever (solid blue), with (a) the coupling along the red dashed line in (c) at 20 µm above the surface, and (b) the coupling versus the height at the position marked by the star in (c), 5 µm outside the pickup loop at X = 15 µm.

that this was a valid simplification to find the general scaling laws concerning the radius of the magnet.

8.6 Enhanced coupling strength to pickup loop

Where traditional MRFM setups utilizing a laser readout of the cantilever motion have a constant detection sensitivity, with our SQUID readout this sensitivity is highly dependent on the position of the magnetic particle with respect to the pickup loop, and on the amplitude of the oscillation of the cantilever. This coupling is obviously very small when the cantilever is far away from the pickup loop, as is the case when we are still determining the exact position of the cantilever. A bit less obvious is the fact that the coupling also becomes small when the magnet is very close the surface of the detection chip. This is because the vertical component of the magnetic field from the magnet is zero in the horizontal plane crossing the magnet. Both of these situations with low coupling should be improved by the second magnet: In the far-field limit the second particle increases the total magnetic moment and thereby the coupling, and close to the pickup loop, when the bottom magnet is nearly touching the surface of the chip, the top particle is still high above the pickup loop with a strong coupling.

These intuitive ideas are checked by a calculation of the coupling from both particles using the equations outlined in Sec. 2.2. The result is shown in Fig. 8.5. The coupling at large distances from the pickup loop (20 μm above the pickup loop) is shown in Fig. 8.5(a), where we find that the ratio between signals of the single and double magnet cantilever is simply equal to the ratio of the volumes of the magnets, since to first order the coupling is proportional to the magnetic moment $m = V\frac{B_\mathrm{r}}{\mu_0}$, with B_r the saturation magnetization. Fig. 8.5(b) shows the coupling versus the height at a typical position where an MRFM experiment could be performed. While it is clear that the coupling for the single magnet decreases rapidly as the height of the magnet is reduced, the coupling of the double magnet to the pickup loop keeps rising, with a maximum increase in coupling of a factor of 3.

We can get some intuition about these values for the coupling by looking at the signals that we would get from the thermal motion of the cantilever. A cantilever with spring constant $k_0 = 80$ μN/m at a temperature of 20 mK has a mean thermally driven amplitude of about 50 pm. In order to be able to detect the thermal motion, this motion has to be multiplied by the coupling strength, and then compared to the SQUID flux noise floor of about 1 $\mu\Phi_0/\sqrt{\mathrm{Hz}}$, while taking into account that we only have about 3% of efficiency in transferring the signal from the pickup loop to the SQUID (see Sec. 2.2.1). So, a detection noise of 1 $\mu\Phi_0/\sqrt{\mathrm{Hz}}$ at the SQUID means a detection limit of about 30 $\mu\Phi_0/\sqrt{\mathrm{Hz}}$ at the pickup loop. This implies that the coupling has to be larger than

$$\frac{30\ \mu\Phi_0}{50\ \mathrm{pm}} = 0.6\ \mathrm{m}\Phi_0/\mathrm{nm} \tag{8.14}$$

for the thermal motion to be detectable within a 1 Hz bandwidth.

8.7 Spin-induced dissipation

We will now present experimental data demonstrating that the new double-magnet cantilevers work, i.e. retain their magnetization, based on measurements of the spin-induced dissipation of the cantilever when coupled to the 2D spin system on the surface of a silicon substrate. This experiment was first performed by Den Haan et al. using a force sensor with a single magnet[77]. In Ref. [77], it is described how the coupling between paramagnetic spins and the magnet on the cantilever opens a dissipation channel for the energy in the cantilever, inducing a shift of the inverse quality factor given by:

$$\Delta\frac{1}{Q} = C\frac{2\pi f_0 T_1}{1 + (2\pi f_0 T_1)^2}, \tag{8.15}$$

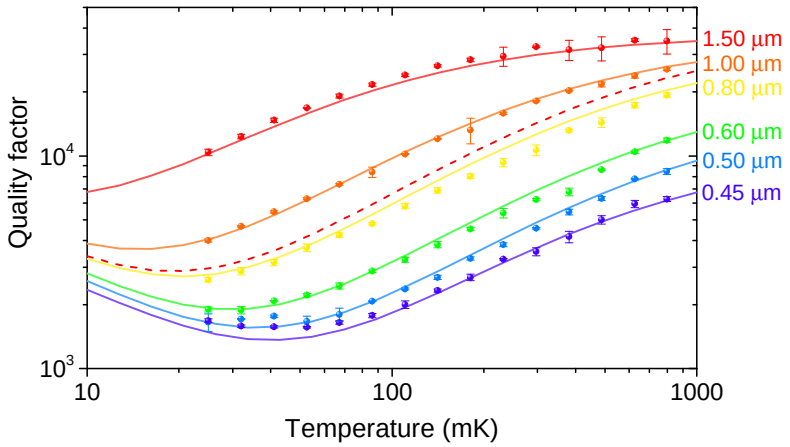

Figure 8.6: Quality factor versus temperature for the new double-magnet cantilever coupled to the electron spins on a silicon substrate. The solid lines are fits to the data for a collective spin density σ and relaxation time T_1. Q_0 is extrapolated from the high temperature limit for each height individually. The dashed red line shows the results of a calculation for a 3.4 µm diameter magnet at $h = 1.5$ µm for identical parameters.

with

$$C = \frac{\sigma\mu^2}{k_0 k_\mathrm{B} T} \int_S \frac{\left(\hat{\boldsymbol{B}}(\boldsymbol{r}) \cdot \frac{\partial \boldsymbol{B}(\boldsymbol{r})}{\partial x}\right)^2}{\cosh^2\left(\frac{\mu B(\boldsymbol{r})}{k_\mathrm{B} T}\right)} d^2\boldsymbol{r} \tag{8.16}$$

The quality factor of the cantilever is then given by $Q^{-1} = Q_0^{-1} + \Delta Q^{-1}$. Using this theory, Den Haan et al. were able to extract a spin density of 0.14 spins/nm^2, with a spin-lattice relaxation time $T_1 = 0.39$ ms.

We have repeated this experiment with the double-magnet cantilever shown in Fig. 8.2 positioned above one of the silicon detection chips. The measurement consists of measuring the properties (resonance frequency and quality factor) of the cantilever for various temperatures and heights above the surface, in our case by performing frequency sweeps around the cantilever resonance frequency using a piezoelectric element to drive the cantilever. The resulting quality factor measured in this experiment is shown in Fig. 8.6. During this experiment, some unintended charging of the cantilever tip or sample induced large 1/f frequency noise, leading to sudden jumps in the cantilever resonance frequency every couple of minutes. For this reason, we were unable to obtain reliable frequency shift data. The 1/f noise does not influence the measurement of the cantilever quality factor, as long as no frequency jump occured during the sweep.

The solid lines in Fig. 8.6 are fits to Eq. 8.15, assuming a magnet with a radius of 0.95 μm and a saturation magnetization of 1.15 T. We cannot extract independent values for the spin density and relaxation time, as this requires reliable frequency shift data. When only the quality factor data is available, the two parameters can balance each other. However, in the limit of $\omega_0 T_1 \ll 1$, the shift of the inverse quality factor is proportional to σ/T_1, so this factor is still a meaningful way to compare the dissipative properties of various surfaces. For the data presented in Fig. 8.6, we find $\sigma/T_1 = 1.04$ $\mathrm{nm^{-2}ms^{-1}}$, a value three times higher than what was reported by Den Haan et al., indicating that the surface of the used detection chip was contaminated, most likely caused by residue of e-beam lithography resist on the surface of the chip. However, considering the poor quality of the surface, the smaller magnets indeed lead to less dissipation of the energy in the cantilever for equal heights, as visible when comparing the solid red line in Fig. 8.6 with the dashed red line, which indicates the calculated quality factor using the same parameters as the other curves but for a magnet with a radius of 1.7 μm.

In the analysis of this data, we have made the following assumptions:

- The minima of the dissipation curves can be used to calibrate the height or saturation magnetization of the magnet. We had to add 300 nm to the assumed height to match the data with the calculations. This height error can be caused by a systematic error in our height calibration method[6], or by a dead layer of the magnet, which reduces the effective radius and then requires a higher saturation magnetization. We believe the problem lies in the height calibration, as the MRFM experiments described in Ch. 4 showed a similar height mismatch.
- Q_0 has been determined individually for each height curve, by extrapolation of the data to high temperatures using that the spin-dependent dissipation has a $1/T$ dependence for high T. We find a quality factor of over 37 000 for the largest heights, and a gradually decreasing quality factor as the height decreases. We attribute this temperature-independent dissipation to the fluctuating charges at the cantilever frequency, whose low frequency counterparts are held responsible for the 1/f frequency noise.

The results from Fig. 8.6 suggest big improvements in the quality factor close to the sample when using smaller magnets. This is made more explicit in Fig. 8.7(a), where we show the calculated spin-induced dissipation for the cantilever coupled to

[6]The height calibration consists of a touch measurement, where the cantilever is slowly approached to the surface until it's motion cannot be detected anymore. Errors can be introduced when, for instance, charging causes the cantilever to bend when close to the sample, or when the cantilever is not aligned perfectly perpendicular to the surface of the detection chip.

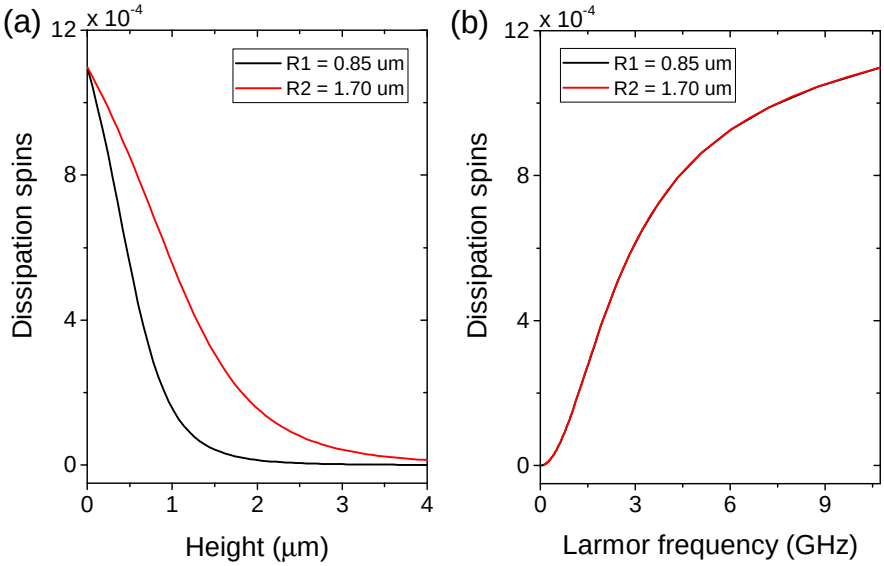

Figure 8.7: Calculation of the spin induced dissipation ($= \Delta Q^{-1}$) using the parameters found in Fig. 8.6 for two different magnet radii, plotted versus (a) the height above the sample and (b) the Larmor frequency of the electron spins in the field from the two magnets.

a 2D spin system at a temperature of 30 mK as a function of the height. However, this presentation of the data is misleading since this compares equal heights. In reality, when using a smaller magnet the experiments have to be performed at smaller distances. Therefore, a better comparison is by looking at constant Larmor frequencies instead, as shown in Fig. 8.7(b). The translation between height and Larmor frequency was done by calculating the magnitude of the magnetic field directly below the magnet for all heights.

We find that the spin-induced dissipation presented in this way is completely independent of the radius of the magnet. This can be understood following the same arguments we used in Sec. 8.3. The dissipation per spin is determined by the square of the field gradient, which is roughly proportional to R_0^{-2} when evaluated at a constant Larmor frequency[7]. At the same time, the total number of spins for a 2D system scales as R_0^2, so the increasing dissipation per spin is perfectly balanced by the decreasing number of contributing spins, making the total dissipation independent of the radius of the magnet.

Note that this finding is only valid when the dissipation originates from a 2D system. In the case that the dissipation originates from the bulk of the sample a

[7] This is equivalent to using a height proportional to the radius.

smaller magnet will lead to reduced dissipation proportional to the radius, and thus a higher quality factor.

8.8 Conclusions

To summarize, we have succeeded in the fabrication of MRFM cantilevers with two magnetic particles, one at the end of the tip with a small radius to generate large field gradients, and a second larger particle several micrometers higher on the cantilever to reduce the detection noise. Initial experiments measuring the spin-induced dissipation show that the new cantilevers are fully functional and should be suited for MRFM experiments. To date, the true MRFM experiments have yet to be done.

With the enhanced field gradients, more sensitive MRFM experiments become possible. In Ch. 4, the prospects for these new cantilevers for the imaging of protons is discussed. However, one should keep in mind that even though the signal per spin increases, the total signal is decreased due to the small detection volumes. Furthermore, the issue of a reduced quality factor of the cantilever by the magnetic coupling to an approximately 2D spin-system is not solved by using these new cantilevers.

A follow up to the fabrication of these cantilevers to get even higher field gradients was attempted in collaboration with the Marohn Group from Cornell University. Although some cantilevers were made, unfortunately they broke before they could be tested in our MRFM setup [205].